CONF-861114--31

EMITTANCE STUDIES OF HIGH INTENSITY NEGATIVE ION SOURCES EQUIPPED WITH CONTINUOUS SURFACE CYLINDRICAL AND SPHERICAL GEOMETRY TUNGSTEN IONIZERS*

G. D. Alton, J. W. McConnell, S. Tajima†, and G. S. Nelson‡
Oak Ridge National Laboratory
Oak Ridge, Tennessee 37831-6373, USA

CONF-861114--31

DE87 003011

A digitally controlled emittance measurement, data acquisition and processing system has been designed, implemented and used to determine emittances of negative ion beams extracted from high-intensity negative-ion sources equipped with cylindrical and spherical geometry cesium surface ionizers. Comparative studies indicate that the emittances of ion beams extracted from the source equipped with a spherical geometry ionizer are lower by 13% to 21% than those extracted from the source equipped with a cylindrical geometry ionizer. This difference may be attributable to geometric factors rather than differences in the sizes of the emission areas at the points of negative-ion generation. Studies reveal that the emittances of these sources are independent of ion mass for most of the materials investigated and independent of ion current over the range of ion currents used in these investigations (4 μA to 12 μA).

*Research sponsored by the Division of Basic Energy Sciences, U.S. Department of Energy, under contract DE-AC05-840R21400 with Martin Marietta Energy Systems, Inc.

†Guest scientist from the Japan Atomic Energy Research Institute.

‡Oak Ridge Associated Universities Student Research Participant from Gustavus Adolphus College.

1. Introduction

The technology of producing negative ion beams of the species and intensities required for tandem electrostatic accelerator applications continues to grow. Significant advancements have been made during the past few years in terms of the intensity capabilities and ion beam qualities (emittances, brightnesses) of sources based on the sputter principle [1]. A number of high intensity, single aperture sources have been described in the literature [2-8] including the sources which are subjects of the present report [7,8]. In such sources, the material of interest is mounted on a negatively biased probe which is typically maintained at potentials of 1-5 kV with respect to housing in a controlled vapor flux of a Group IA element, usually cesium. A fraction of the vapor, ionized by direct surface ionization from a hot surface or by electron impact plasma discharge ionization, is used to sputter the sample surface. Cesium is most commonly used in such sources because it has the lowest first ionization potential of the Group IA elements (3.89 eV); as an adsorbate, cesium also effects the greatest changes in work function and thus is the most effective of the Group IA elements in forming negative ions through surface ionization processes [9]. Negative-ion sources based on the sputter principle all share in common the influences of the intrinsic energy and angular distribution characteristics of the sputter process [10] on the quality of extracted negative-ion beams. However, emittances and brightnesses of beams extracted from such sources may also differ significantly depending on the method employed and the geometry used for positive ion formation. Other geometrical factors may also affect the size, shape and angular distribution characteristics of the sputter-eroded negative-ion generation surface and hence

the intensity and quality of the extracted negative-ion beam.

To date, high-intensity negative-ion sources based on the sputter principle have utilized either electron impact plasma discharge [2,3] or direct surface ionization by a hot surface [4-8] to ionize the cesium vapor. In the plasma discharge source, cesium ions, extracted from the plasma column, bombard a spherical sector cathode more or less uniformly; negative ions ejected in the sputter process are accelerated across the plasma sheath and focused by the spherically symmetric plasma sheath/electrode system at an aperture positioned at the locus of the radius of curvature of the cathode surface. Because of the spherical symmetry, the electrode system is, in principle, aberrationless and therefore the beam quality should be dominated principally by the energy and angular distributions of the sputter process. (Of course, other factors contribute to the measured emittance of an ion source such as space charge effects and aberrations induced by the extraction and beam transport lensing devices and momentum analysis system.) Sources of this type are often referred to as radial geometry Penning discharge sources due to the fact that negative ions are extracted in a radial direction with respect to the column plasma discharge axis. Emittance and brightness measurements for this source type have been made by Tykkesson, Andersen, and Heinemeier [11].

In sources which utilize surface ionization to produce the positive ion beam such as those described in this report, the ionizer is made of a high work function material such as Ta or W which is maintained at ~1100°C and placed in axial alignment with the sputter probe in an inverted configuration. Cesium atoms which impinge on the surface may be ionized with unit efficiency provided that ions can be extracted as fast as they are

evaporated from the hot surface. Space charge effects, however, may reduce the efficiency of the ionization process. Cesium ions evaporated from the ionizer surface are accelerated by the potential difference maintained between the negatively biased probe and ionizer where they effect a sputtering of the material of interest. The positive ion current density distribution on the sample surface which defines the negative ion generation region is determined by the ionizer geometry and the potential distribution within the ionizer/sputter probe region. Initially, the negative-ion current density distribution is expected to follow that of the positive ion beam, neglecting surface saturation effects. After sustained ion bombardment, an erosion crater will be formed, the size and shape of which determines the negative-ion generation surface and the angular distribution of sputter-ejected particles; it also alters the potential distribution near the sputter probe surface and hence alters the angular distribution through optical effects near the surface.

Several types and shapes of surface ionizers have been employed in this source type including spiral-wound-wire cylindrical [4-6] and continuous-surface cylindrical [7] and spherical geometries [8]. The most frequently used ionizer materials are Ta and W. The sources described in this report utilize continuous surface cylindrical and spherical geometry tungsten ionizers which produce small, azimuthally symmetric, radially-graded sputter erosion patterns during the negative-ion generation process. Sources employing spiral-wound-wire ionizers usually exhibit larger radially-graded, azimuthally-asymmetric sputter-erosion patterns due to the nature of the ionizer surface -- a characteristic which should increase the emittances of sources equipped with this type of ionizer. In this report,

we describe the device and techniques utilized and the results derived from studies of the emittances of ion beams extracted from sources equipped with continuous surface cylindrical and spherical geometry ionizers.

2. Definitions

Liouville's Theorem. The quality of an ion beam is usually expressed in terms of emittance ε and brightness B. Both are related and are direct consequences of Liouville's theorem, which postulates that the motion of a group of particles under the action of conservative force fields is such that the local number density in the six-dimensional phase space (hypervolume) x,y,z,p_x,p_y,p_z everywhere remains constant. An ion beam, therefore, can be represented by a group of points, all points of which lie within the six-dimensional hypervolume.

Emittance. If the transverse components of motion of a group of particles are mutually independent in configuration space (i.e., neglecting space charge and spin-dependent interactions), the motion of the particles in orthogonal places (x,p_x), (y,p_y), and (z,p_z) will be uncoupled and therefore can be treated separately. For a beam moving in the z direction under the action of conservative forces, the four-dimensional hyperarea (x,p_x,y,p_y) is a conserved quantity.

For the case where p_z is constant, the transverse momenta p_x,p_y can be replaced by corresponding angular components, since

$$\frac{p_x}{p_z} = \tan \theta_y \cong \frac{dy}{dz} = y' \tag{1}$$

and

$$\frac{p_x}{p_z} = \tan \theta_x \cong \frac{dx}{dz} = x' \tag{2}$$

in the small angle approximation. The respective transverse phase space areas then are proportional to the areas (x,x') and (y,y').

To account for changes in the axial momentum p_z of an ion beam, the concept of normalized emittance is often used. We define the orthogonal normalized emittances as

$$\varepsilon_{nx} = \pi x x' \sqrt{E} \tag{3}$$

and

$$\varepsilon_{ny} = \pi y y' \sqrt{E} \tag{4}$$

where E is the energy of the ion beam. The units of emittance are often given in terms of $\pi \cdot mm \cdot mrad\ (MeV)^{1/2}$.

Brightness. Another figure of merit often used for evaluating ion beams is the brightness B. Brightness is defined in terms of the ion current dI per unit area dS per unit solid angle $d\Omega$ or

$$B = \frac{dI}{dS\ d\Omega} \tag{5}$$

where $dS\ d\Omega$ can be related to the normalized emittance [12] by

$$dS\ d\Omega = \varepsilon_{nx}\varepsilon_{ny}/2 \tag{6}$$

$$B = \frac{2dI}{\varepsilon_{nx}\varepsilon_{ny}}\ . \tag{7}$$

3. The emittance measuring device

The emittance measurement device consists of a vacuum housing, two identical stepping motor-driven detector units for determining the emittances of an ion beam in either the x or y directions and a control unit for driving the detector hardware [13]. The control unit consists of an IBM personal computer (PC) which is interfaced to a Transiac model 6001 CAMAC-crate controller [14], an input/output register, a stepping motor

controller, and a 12 bit analog-to-digital converter (ADC). The CAMAC crate control modules communicate with the emittance measurement hardware via an external electronics unit. The electronics unit consists of a relay unit for x,y direction selection, fast switches for stepping motor brake control, a current-to-voltage converter for processing detector current signals, current range logic circuitry, current integrators and an analog multiplexer. A block diagram of the control system electronics is shown in fig. 1.

The ion beam diagnostic unit (fig. 2) consists of an electrically isolated slit aperture, positioned 0.4 m in front of a detector unit which is made up of 32 electrically isolated plates. The current striking each of the detectors is used to determine the differential angular divergence of the ion beamlet which is allowed to pass through the slit aperture at a given x or y position.

An emittance measurement consists of stepping the slit-detector system through an ion beam in a chosen direction while monitoring the total ion current striking the slit unit and the differential ion currents striking each of the 32 detectors during a fixed integration time period (~5 ms). The position at which data are accumulated is determined by the voltage signal from a precision linear potentiometer. The ion currents from the slit unit and each of the 32 detection plates are converted to voltage signals and, along with the position voltage signals for each of 50 positions, are digitized and stored as a file on hard disk. The data set can be called from file for data analysis. A complete set of x or y data, including background data, can be acquired and stored in memory in less than 5 minutes. An additional 20 minutes is required to process the data and

extract emittance values. Modifications to the control program and electronics unit permit measurement of emittances of negative-ion beams extracted from negative-ion sources operated in pulsed mode.

Data Analysis. Prior to data storage or analysis, a menu selectable option permits a three-dimensional monitor display of the xx′ or yy′ versus intensity data set. By visually inspecting the raw data, a decision can be made whether to keep or erase the particular data file. If the data set is considered worthy of keeping, it is, first of all, subjected to point-by-point background subtraction by use of a background data file taken immediately after the beam measurement. This procedure is necessary because of the difficulty of electronically reducing the residual background to zero in each of the 32-detector channels. In order to compensate for variations in beam intensity during a particular measurement, the data set is then normalized by multiplying each of the 32-detector-channel readings by the ratio of the maximum slit current reading to the slit current reading at each of 50 positions. The data set is then ready for extraction of emittance information. By selecting the appropriate option, emittance contours are calculated and automatically plotted. The contour levels are determined by performing a Simpson's rule volume integration over the xx′ or yy′ versus intensity data set. Contour levels which contain 10% through 80% of the total beam are calculated iteratively in increments of 10% to an accuracy of 0.1%. The contour level information is then passed to a topographical graphics program which produces contour plots from the data. The area within a particular contour is just the emittance for this particular beam fraction.

4. Negative-ion source descriptions

The negative-ion sources which were used in the emittance measurements described in this report have been described in detail previously [7,8], and therefore only a very brief account of their principles of operation will be given here. The sources were designed in 1981 and are second-generation developments of a similar source designed and developed in 1978 [5]. These sources, however, possess significantly improved mechanical design features; both sources also exhibit very different performance characteristics. These sources, like other sources which have been developed in recent years [2-6], utilize the technique of secondary ion yield enhancement by sputtering a sample containing the material of interest in the presence of minute amounts (< 1 monolayer) of Group IA elements [1]. The sources described in this report utilize continuous surface solid tungsten cylindrical [7] or spherical geometry ionizers [8]. The spherical geometry source is similar to that proposed by White [15]. Simple continuous ionizer surfaces offer well-defined boundaries for positive ion generation which are more amenable to computer simulation than those associated with more complex emission surfaces. More importantly, negative-ion yields from the surface surrounding the usual axially located, concentrated sputter erosion pattern on the probe appear to be considerably lower than those associated with helically wound ionizers. This beam is often referred to as a halo beam. The halo effect is reduced to almost zero in the spherical geometry ionizer source. In these sources, only ions generated from the desired surface of the ionizer are accelerated; all other heated surfaces are obscured from the electric field region of the ionizer/sputter probe electrode system. The sputter pattern in the cylindrical geometry

ionizer source exhibits a weakly, uniformly worn area surrounding the concentrated wear pattern located on axis; thus, the halo effect is more pronounced than in the spherical geometry source.

The Cylindrical Geometry Ionizer Source. An example of positive ion trajectories through the ionizer/sputter probe region of the source is shown in fig. 3; the computed ion current density resulting from positive ion impact at the sample surface is shown in fig. 4.

The wear pattern which would result from the positive ion distribution shown in fig. 4 is composed of two parts: a region of concentrated wear with full diameter of ~0.75 mm, and a low density uniform wear region with diameter ~4.5 mm. The negative-ion exit aperture is 4.78 mm in diameter. The probe wear patterns observed in practice are found to closely approximate those predicted from such calculations.

The Spherical Geometry Ionizer Source. An example of computed positive-ion trajectories between the ionizer and sputter sample is shown in fig. 5, and the corresponding positive-ion current density distribution at the sample surface is shown in fig. 6. Note the lack of an appreciable halo surrounding the high current density distribution for this ionizer. The full width of the beam at impact with the sample surface is approximately the same as that of the high current density region in the cylindrical ionizer source (~0.75 mm). Based on the apparently smaller halo, this source should, in principle, have a lower emittance than the cylindrical ionizer geometry source.

5. Emittance measurements

Emittance measurements of the ion beams extracted from the subject

sources were determined by use of the equipment and procedures described in Section 3 of this report. The sources were mounted on a test stand equipped with capabilities for accelerating the negative ion beams up to energies of 30 keV with energies of 20 keV typical of all measurements; a conventional, three-cylinder einzel lens was used to focus the ion beam onto the slit of the emittance detector assembly which was placed in axial alignment with the ion source. The ratio of ion beam to einzel lens diameter during the measurements was ~1:3 and therefore the lens is expected to aberrate the ion beams appreciably. Future plans call for the use of a single gridded einzel lens of larger diameter and much lower aberration coefficients for such measurements. The test stand was not equipped with mass analysis capabilities. However, efforts were made to minimize contributions to the total negative ion current from the source by carefully cleaning the elemental material samples chosen for these investigations prior to installation and then sputter cleaning in the source for extended periods of time (~8-12 hours) until the total negative ion current reached steady state values. This procedure was adopted to remove surface oxides and other contaminants and thereby minimize spurious contributions to the emittance from ion species other than those from the material of interest. When equipped with high electron affinity sputter probes such as those chosen for the present investigations (Ag, Au, Ni and Si), the mass spectra from high intensity negative-ion sources such as those described in this report are usually dominated by the monomer negative-ion species. An exception, in the case of the materials used for these investigations, is Si which produces a rather large dimer negative-ion beam (Si_2^-). During all measurements, the negative-ion currents were controlled by variation of the

sputter probe potential -- all other source parameters were fixed (e.g., ion extraction potential and ionizer and cesium oven temperatures, etc.). Typical examples of the emittance contours (10% through 80%) obtained from an Au sample are shown in figs. 7 and 8. It is interesting to note that the emittance values for the 80% contours agree closely with estimations based on simple geometrical arguments; i.e., the full width of the high density portion of the cesium ion beam at impact with the probe surface (~1 mm) and the angular divergence limitations imposed by the 4.78-mm exit aperture. For example, the estimated emittance value for the source is 53 π•mm•mrad, compared to a measured value for the 80% contour for the "y" direction of 53 π•mm•mrad; similar agreement between measured and calculated values are obtained for the source equipped with a spherical geometry ionizer.

Cylindrical Ionizer Geometry Source Data. Two-dimensional emittances versus percentage of total negative-ion beam (4 μA) extracted from the cylindrical ionizer geometry negative-ion source produced by sputter ion bombardment of Ag, Au, Ni, and Si samples are shown in fig. 9. Under the assumption that the total negative-ion current is made up of the monomer negative-ion species from the sample material of interest, there is no evidence of a monotonic dependence of the two-dimensional emittance on ion mass; these data, therefore, support the findings of Doucas, Hyder, and Knox [16]. However, the emittance values from the Si sample are seen to be consistently lower by ~13% than those for the average values of the other sample materials (Ag, Au, Ni) which were examined.

Spherical Geometry Ionizer Source Data. The results derived from measurements of the emittances versus percentage total negative-ion current

extracted from an Ag sample in the spherical geometry ionizer source for total beam currents of 4, 6, 8, 10, and 12 μA are displayed in fig. 10. Over the range of negative-ion currents investigated, there is no evidence of the rather strong dependence of emittance on negative-ion current as found by Doucas, Hyder, and Knox for ion beams extracted from the cone geometry negative-sputter-ion source [16]. Such increases are most probably attributable to changes in emission area due to changes in the positive ion beam size at impact induced by positive ion beam space charge effects.

Emittance Comparisons. A comparison of the emittance versus percentage total negative ion beam extracted from the two sources is made in fig. 11. The samples used during these measurements were Ag; the total negative ion currents were maintained at 4 μA. Based on the results shown in fig. 11 and those displayed in figs. 9 and 10, the emittances from the spherical geometry ionizer source are consistently 13% to 21% lower than those from the cylindrical geometry source at the same percentage total current level. These results complement arguments made earlier which were based on the presence or the lack thereof of a halo beam in the cesium ion impact area of the sample probe. However, since both sources were equipped with ion exit apertures of diameter ϕ = 4.78 mm, the half angles defined by a point on the axis of the sample probe and the aperture are slightly different. The half angle for the spherical geometry ionizer source is lower by ~13% than that associated with the cylindrical geometry source. The differences in emittances could be partially or totally attributable to this aperture effect. The agreement between measured emittance for the 80% contour and estimated values based on the geometrical arguments discussed previously support the latter conjecture.

6. Discussions and conclusions

These measurements suggest that the emittance of ion beams extracted from the source equipped with a spherical geometry ionizer are lower by 13% to 21% than those extracted from the source equipped with a cylindrical geometry ionizer. The agreement between measured emittances and emittances estimated using simple geometrical arguments suggest that differences in emittance of the source may be attributable to geometrical rather than fundamental factors such as the presence or lack thereof of a halo surrounding the high density cesium impact region of the sample probe. The emittances of ion beams extracted from the cylindrical geometry source are found to be independent of mass for ion beams generated from Ag, Au and Ni samples; on the other hand, the emittances from Si probes were found to be consistently lower by ~13% than those from Ag, Au and Ni samples. In contrast to the findings of Doucas, Hyder, and Knox [16] for the emittances of beams extracted from the cesium sputter cone-type source, the emittances of ion beams extracted from the spherical geometry ionizer do not increase with increasing negative-ion current over the range of negative-ion currents investigated (4 μA to 12 μA).

The results of these measurements may be influenced by the lack of mass analysis and by the use of an inappropriately designed einzel lens which is expected to aberrate the ion beam. Future emittance studies are planned which will include the use of both mass analysis and a low aberration coefficient lens.

Acknowledgements

The authors are indebted to Ms. Althea Tate for the skillful typing of this manuscript.

References

[1] V. E. Krohn, Jr., Appl. Phys. 33 (1962) 3523.

[2] H. H. Andersen and P. Tykesson, IEEE Trans. Nucl. Sci. NS-22 (1975) 1632.

[3] G. D. Alton and G. C. Blazey, Nucl. Instrum. Methods 166 (1979) 105; G. D. Alton, R. M. Beckers, and J. W. Johnson, ibid., 148.

[4] G. T. Caskey, R. A. Douglas, H. T. Richards, and H. V. Smith, Jr., Nucl. Instrum. Methods 157 (1978) 1.

[5] G. D. Alton, IEEE Trans. Nucl. Sci. NS-26 (3) (1979) 3708.

[6] R. Middleton, Nucl. Instrum. and Meth. 214 (1982) 139.

[7] G. D. Alton, Nucl. Instrum. and Meth., Phys. Res. A244 (1986) 133.

[8] G. D. Alton and G. D. Mills, IEEE Trans. Nucl. Sci. NS-32 (5) (1985) 1822.

[9] G. D. Alton, Surf. Sci. 175 (1986) 226.

[10] R. Behrisch, ed. 1981 Sputtering by Particle Bombardment, Vol. 47 (New York: Springer).

[11] P. Tykkesson, H. H. Andersen, and J. Heinemeier, IEEE Trans. Nucl. Sci. NS-23 (2) (1976) 1104.

[12] T. R. Walsh, J. Nucl. Energy, Pt.C. 4 (1962) 53;
T. R. Walsh, J. Nucl. Energy, Pt.C. 5 (1963) 17.

[13] Nukleartechnik, Gelnhausen-Hailer, West Germany.

[14] Transiac, Inc., Mountain View, CA.

[15] N. R. White, Nucl. Instrum. and Meth. 206 (1983) 15.

[16] G. Doucas and H. R. Mck. Hyder, Nucl. Instrum. and Meth. 119 (1974) 413; G. Doucas, H. R. Mck. Hyder, and A. B. Knox, Nucl. Instrum. and Meth. 124 (1975) 11.

Figure Captions

1. Block diagram for the emittance measurement hardware control and data acquisition system electronics.
2. Schematic drawing of the emittance measurement detector unit.
3. Calculated positive ion trajectories in the cesium ionizer/sputter probe field region of the cylindrical ionizer geometry negative ion source.
4. Calculated positive ion current density distribution at the sputter probe surface of the negative ion source equipped with a cylindrical geometry ionizer.
5. Calculated positive ion trajectories in the cesium ionizer/sputter probe field region of the spherical ionizer geometry negative-ion source.
6. Calculated positive ion current density distribution at the sputter probe surface of the negative ion source equipped with a spherical geometry ionizer.
7. x-direction emittance contours for the negative ion source equipped with a cylindrical geometry ionizer. Ion species: Au^-; beam intensity: 6 μA.
8. y-direction emittance contours for the negative ion source equipped with a cylindrical geometry ionizer. Ion species: Au^-; beam intensity: 6 μA.
9. Emittance versus percentage of total negative-ion beam from Ag, Au, Ni and Si samples. Source: cylindrical geometry ionizer; negative-ion current: 4 μA

10. Emittance versus percentage of total negative ion beam for various negative ion currents. Source: spherical ionizer geometry; ion species: Ag^-

11. Comparison of normalized emittances versus percentage of total negative ion beam for sources equipped with cylindrical and spherical geometry ionizers. Ion species: Ag^-; negative ion current: 4 μA.

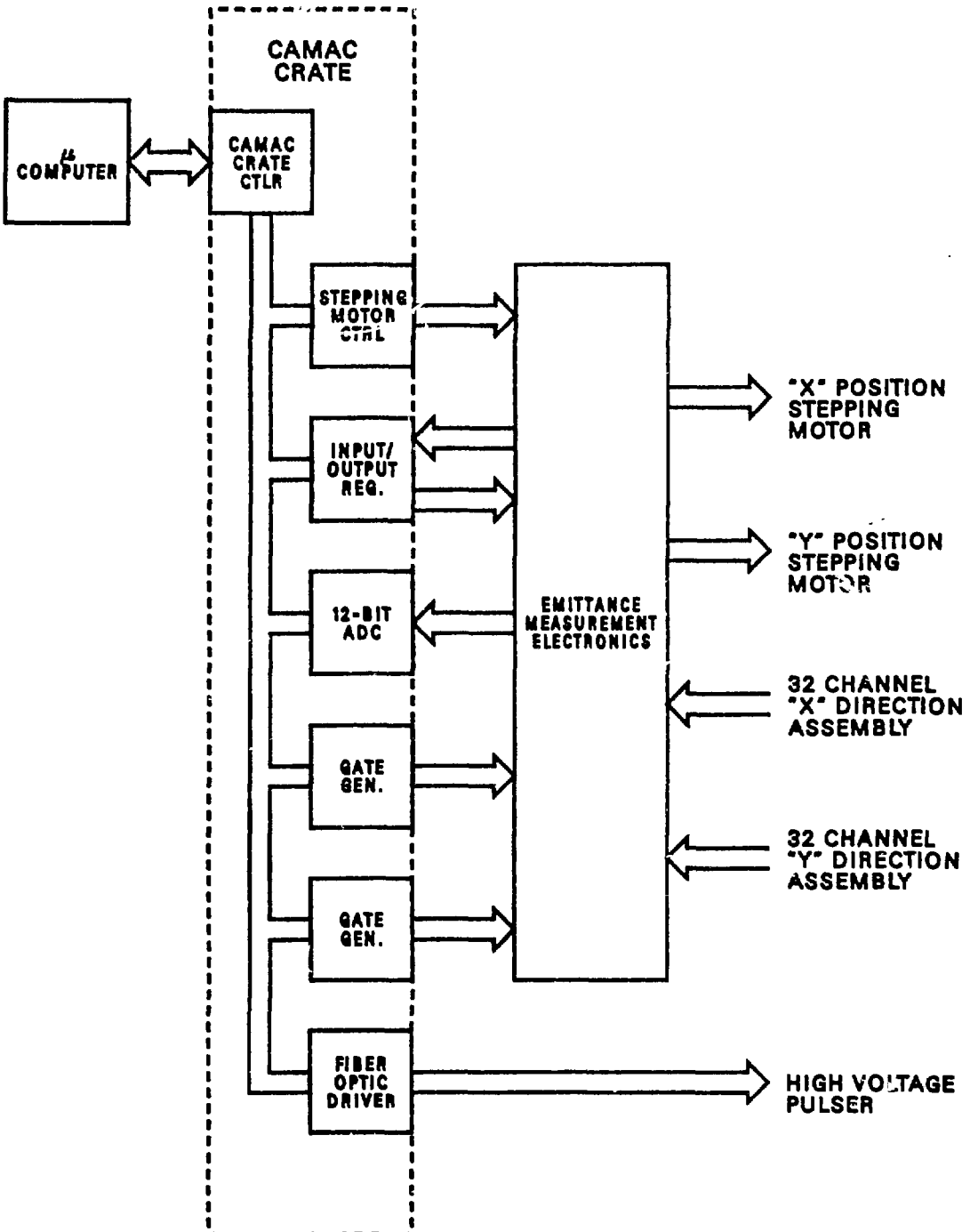
CAMAC CRATE
COMPUTER
CAMAC CRATE CTLR
STEPPING MOTOR CTRL
INPUT/ OUTPUT REG.
12-BIT ADC
GATE GEN.
GATE GEN.
FIBER OPTIC DRIVER
EMITTANCE MEASUREMENT ELECTRONICS
"X" POSITION STEPPING MOTOR
"Y" POSITION STEPPING MOTOR
32 CHANNEL "X" DIRECTION ASSEMBLY
32 CHANNEL "Y" DIRECTION ASSEMBLY
HIGH VOLTAGE PULSER

Fig. 1

ORNL-DWG 76-16444R

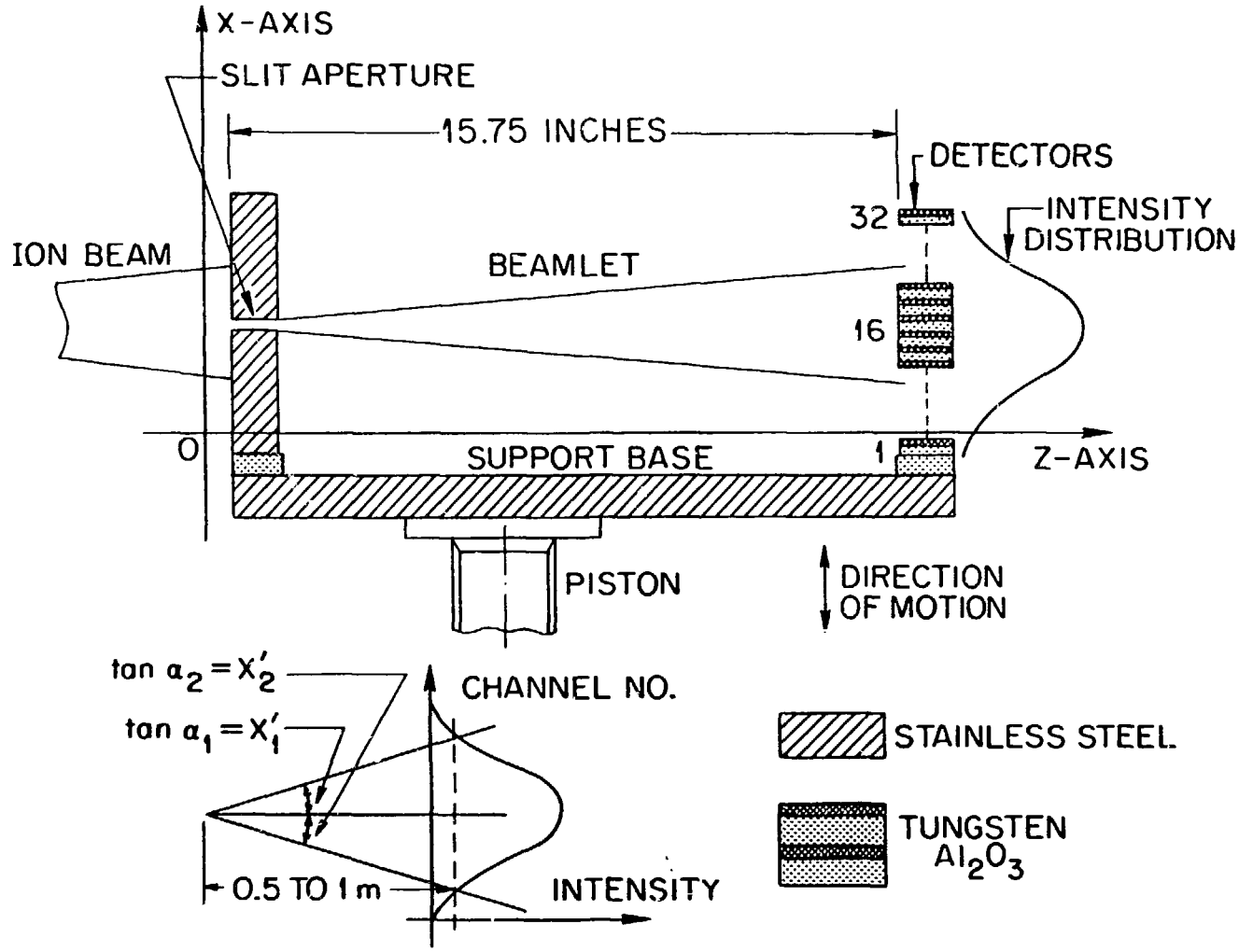

Fig. 2

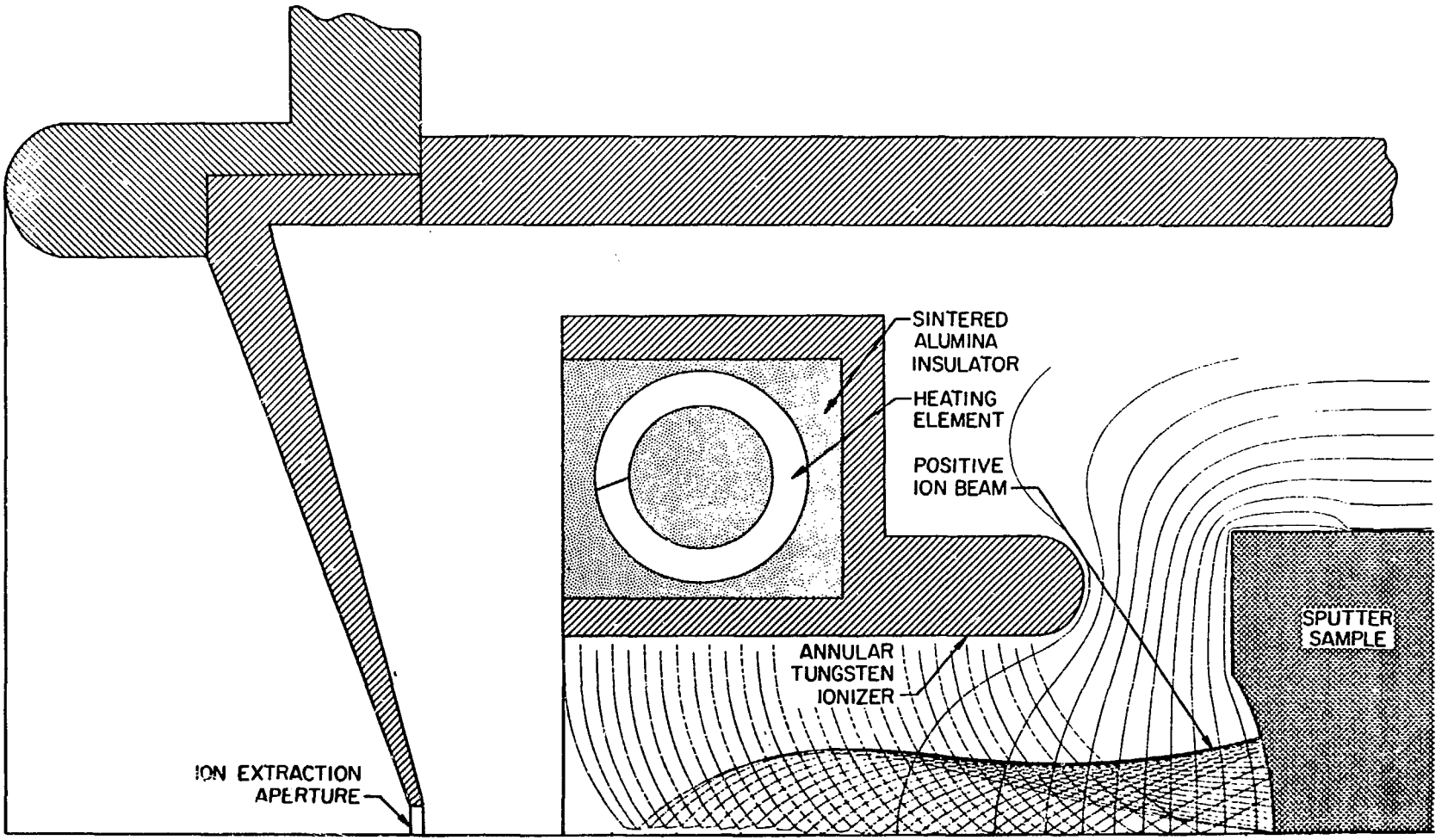
SINTERED
ALUMINA
INSULATOR
HEATING
ELEMENT
POSITIVE
ION BEAM
SPUTTER
SAMPLE
ANNULAR
TUNGSTEN
IONIZER
ION EXTRACTION
APERTURE

Fig. 3

ORNL-DWG 84-16366AR

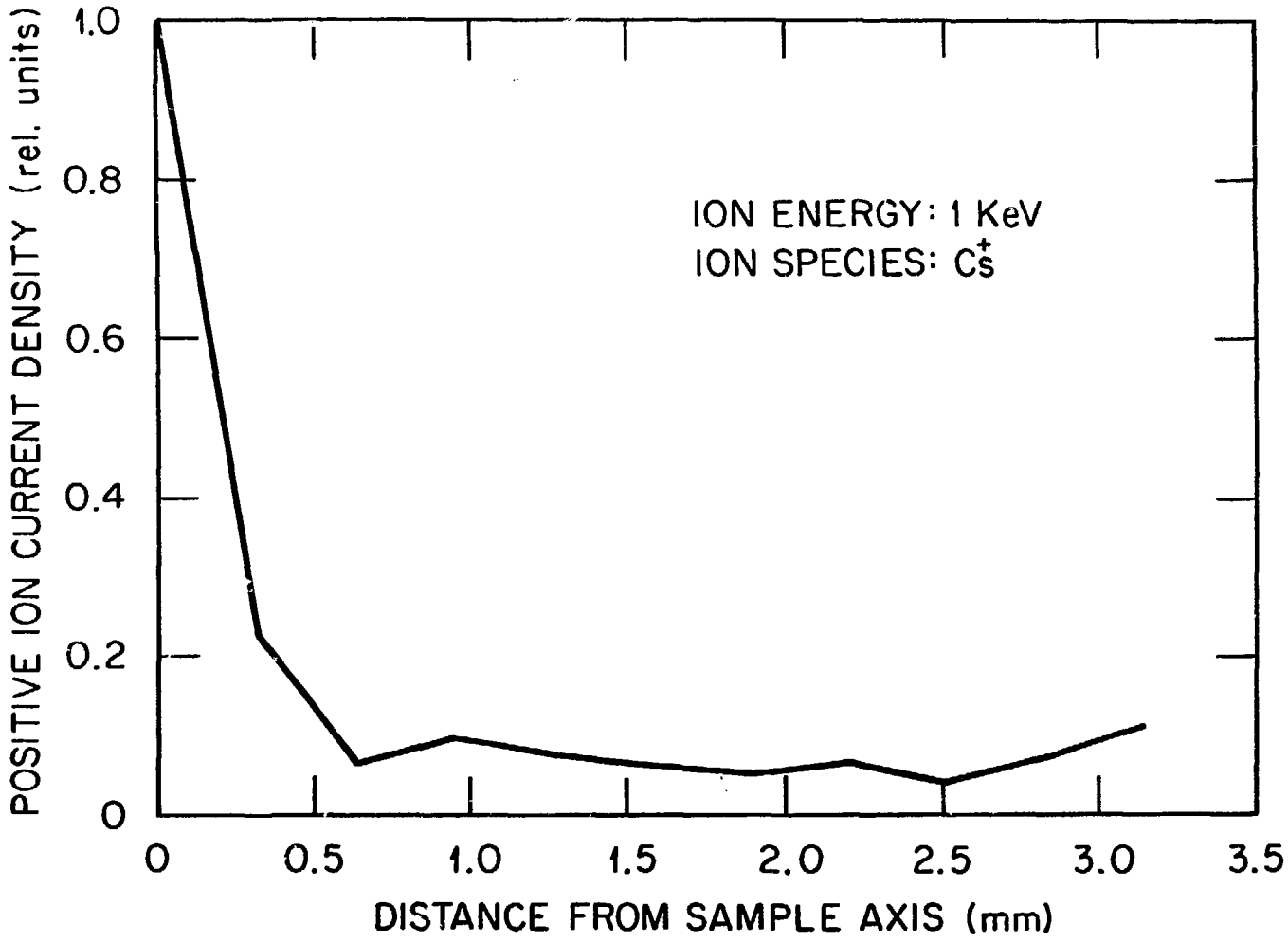

Fig. 4

ORNL-DWG 83-19379R

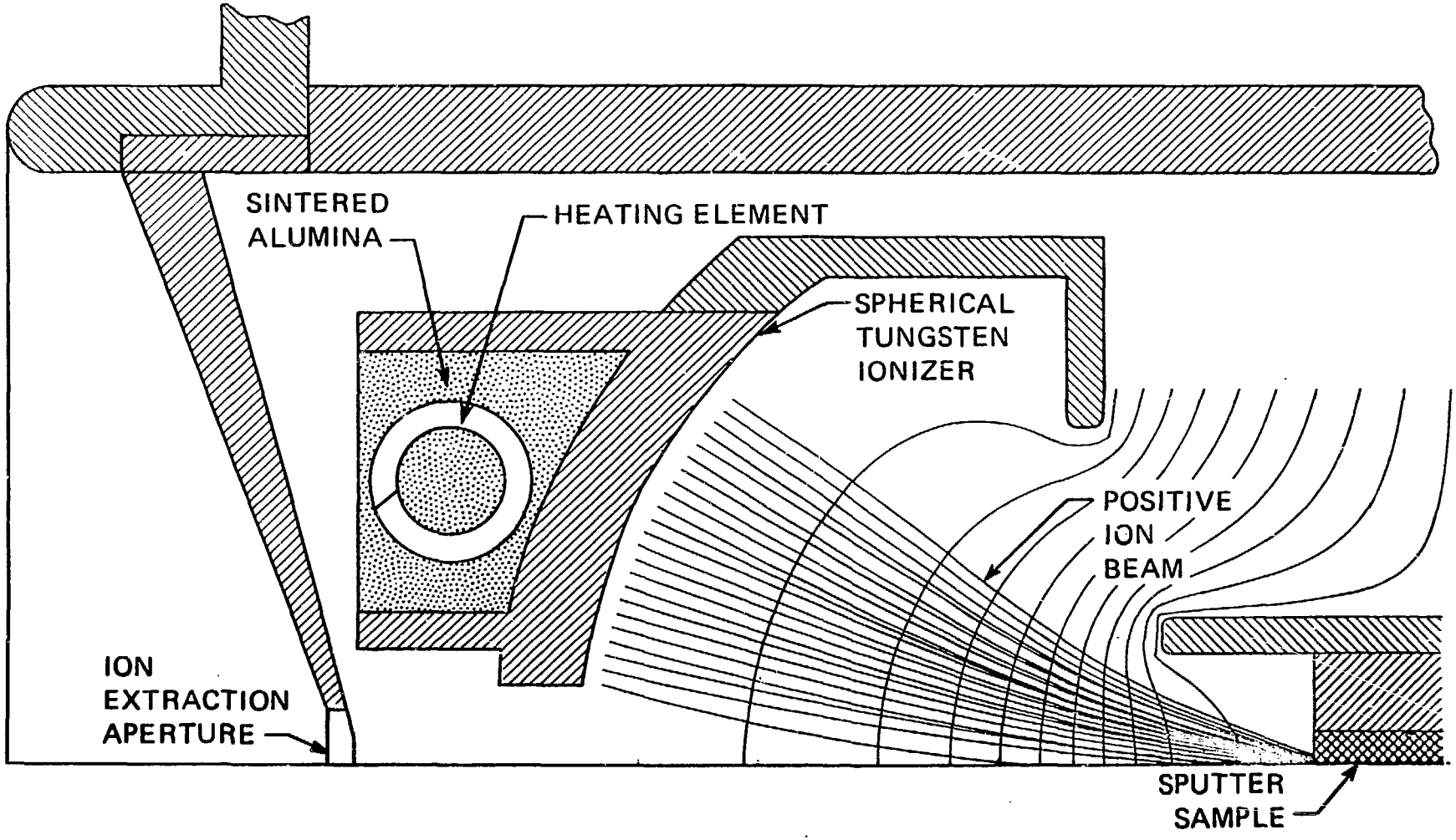

ORNL-DWG 85-9799R

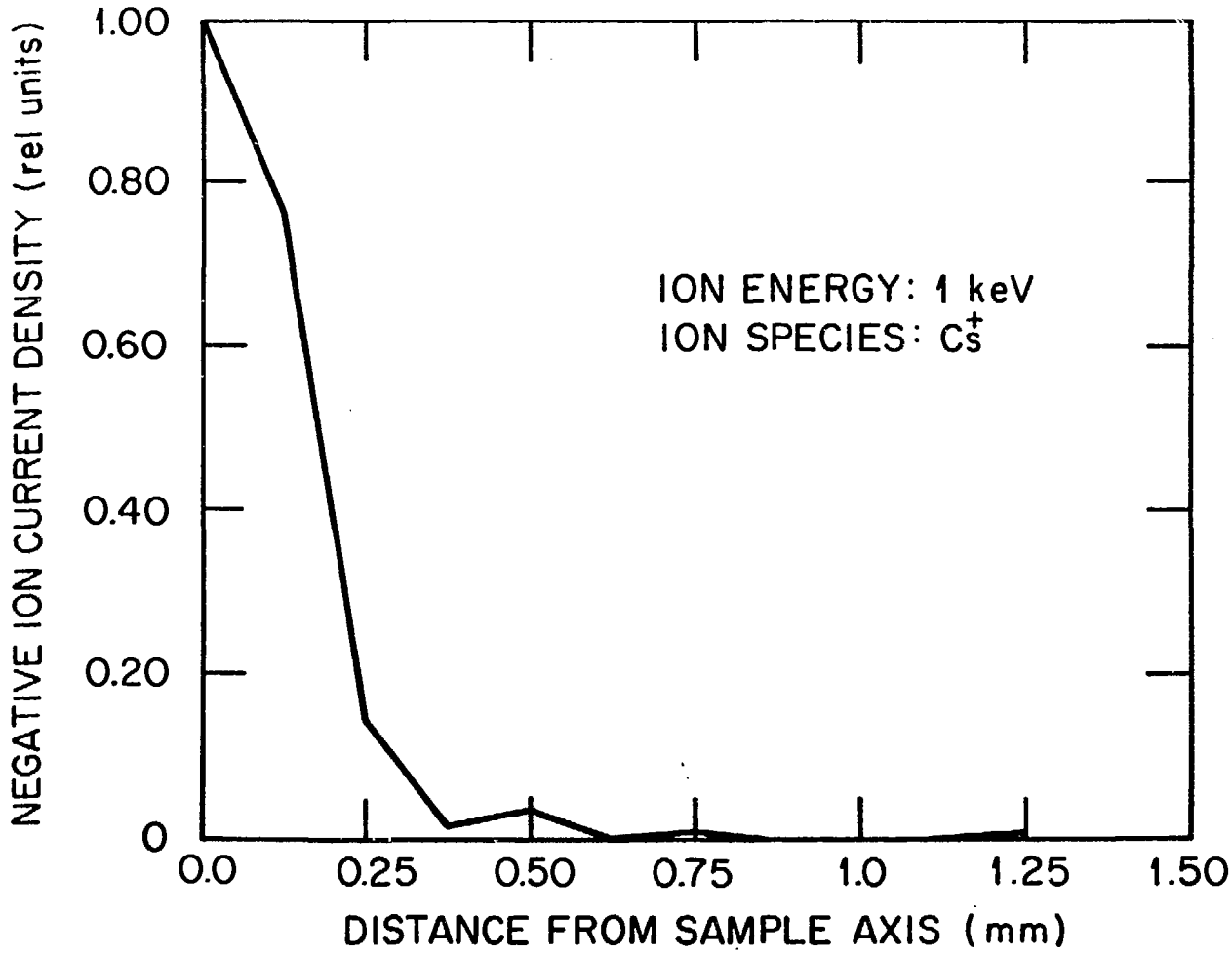

Fig. 6

ORNL–DWG 86-10664

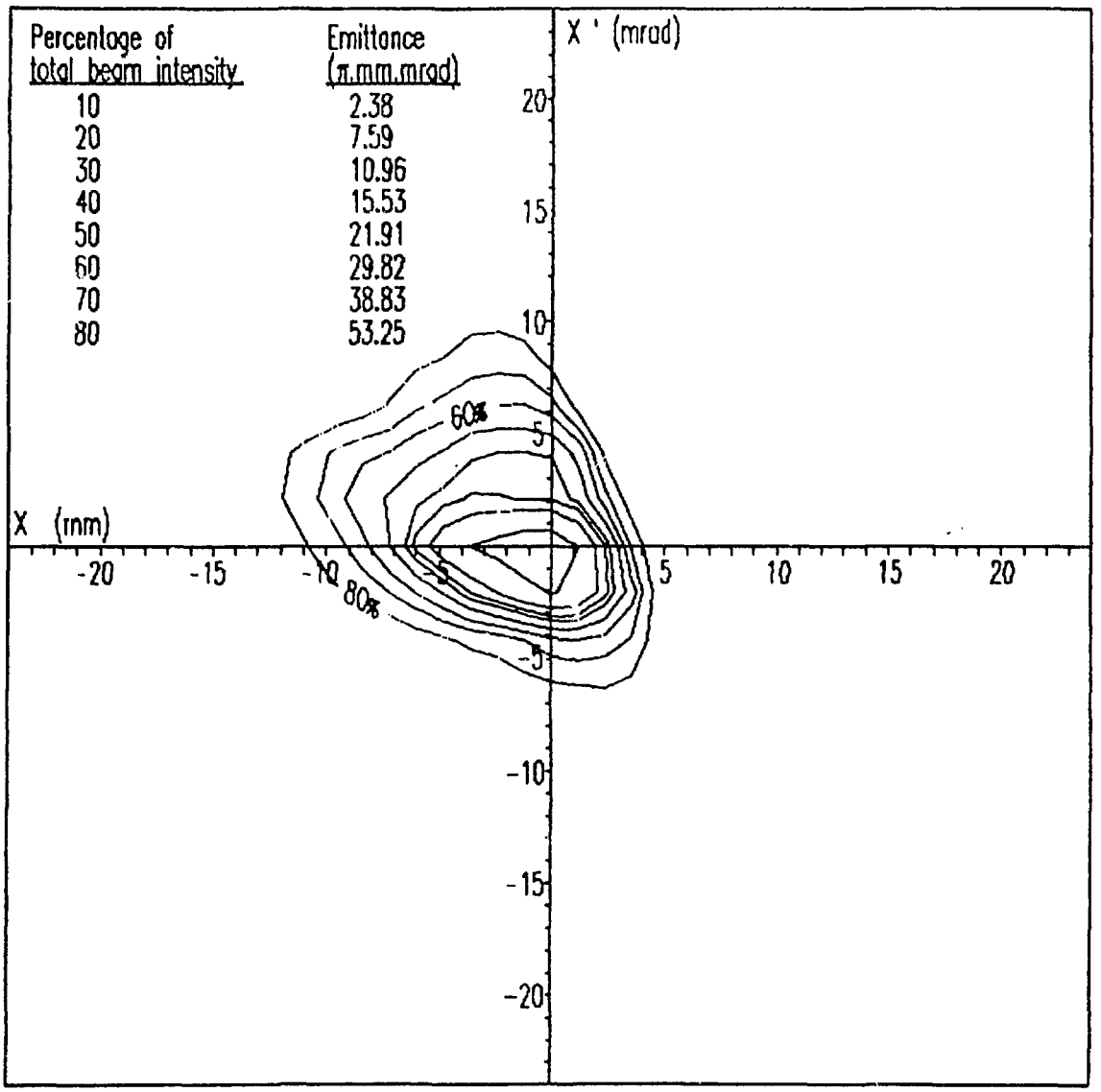

Fig. 7

ORNL–DWG 85-17457R

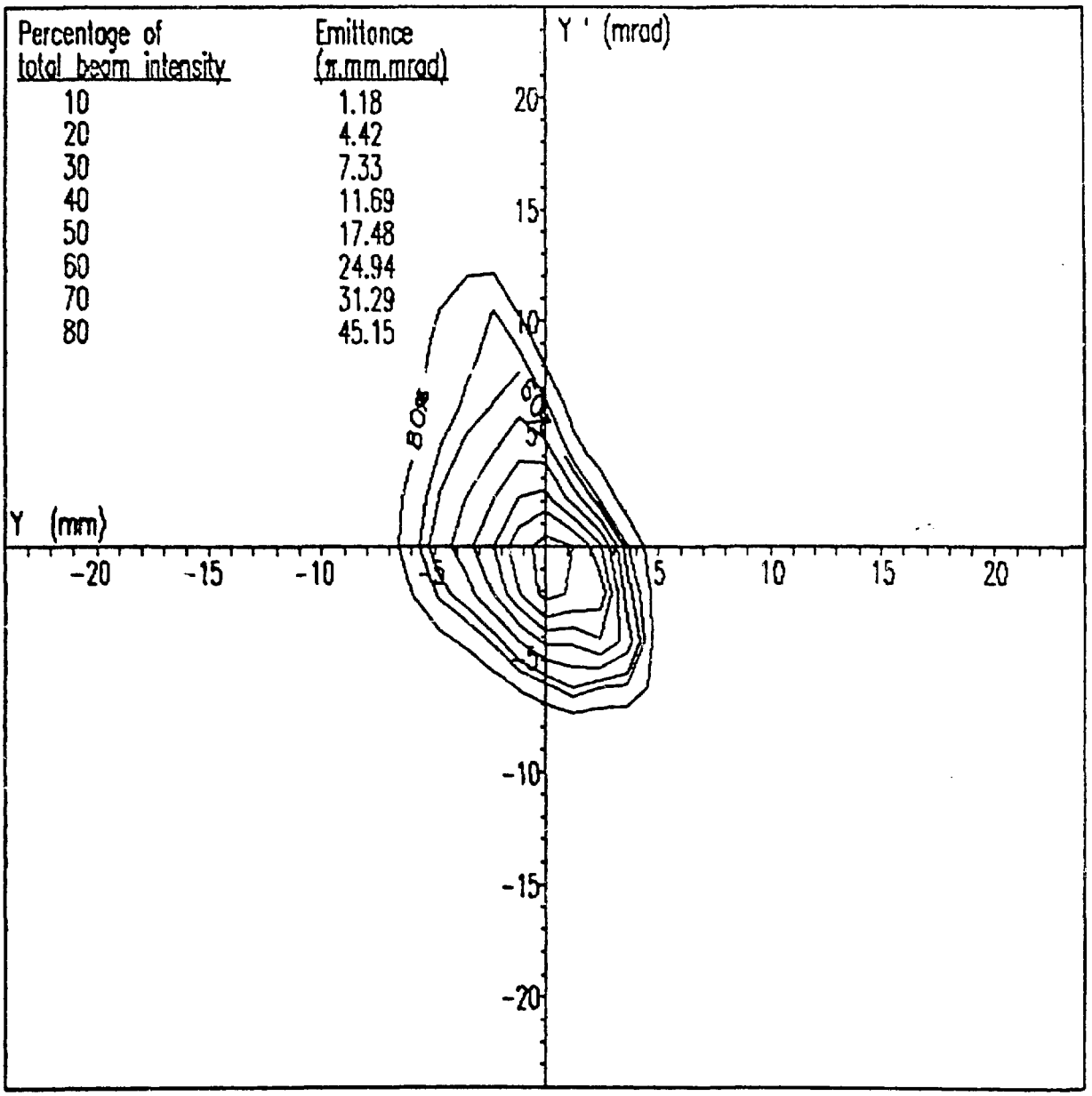

Fig. 8

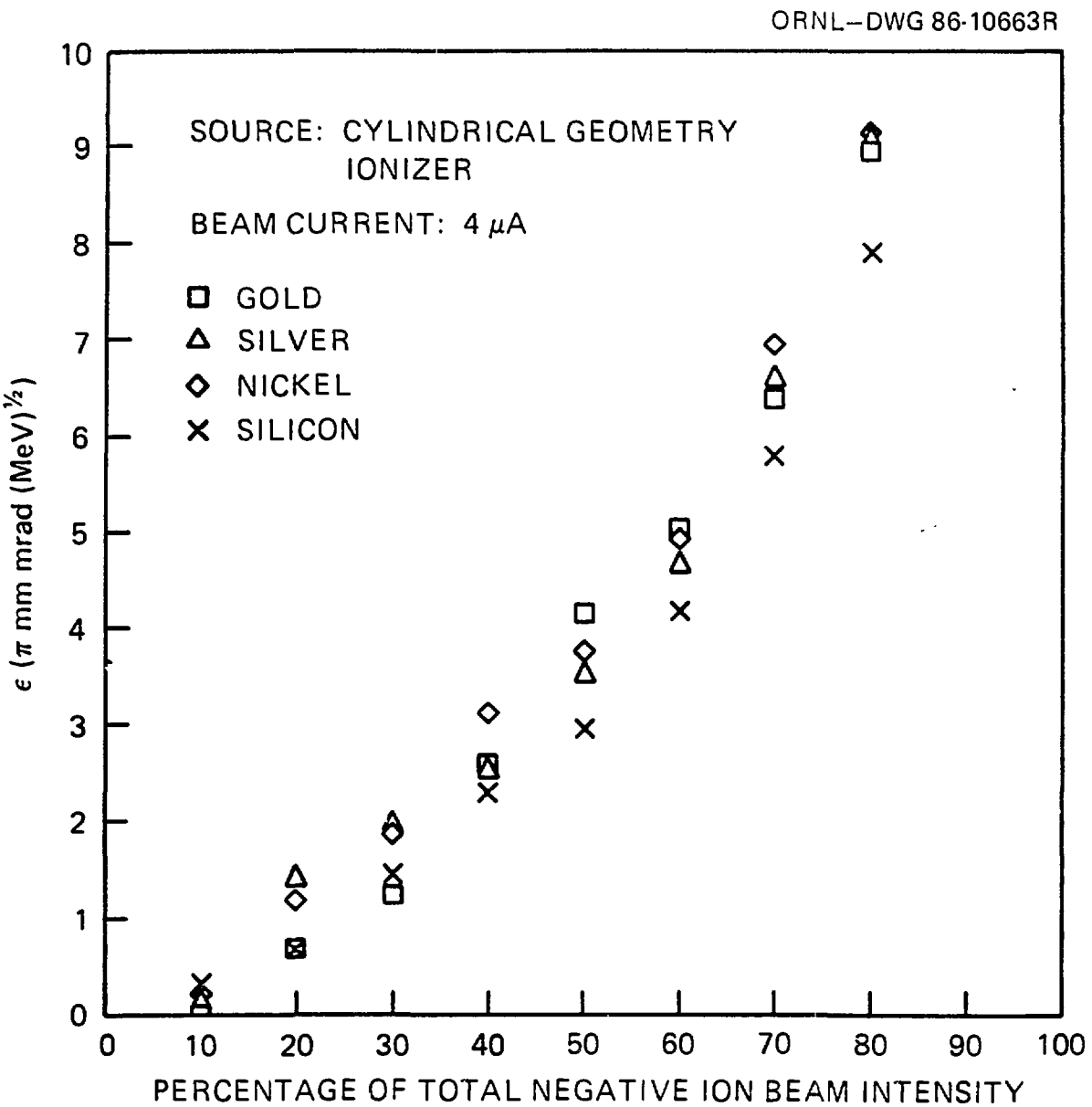
ORNL–DWG 86-10663R
SOURCE: CYLINDRICAL GEOMETRY IONIZER
BEAM CURRENT: 4 μA
GOLD
SILVER
NICKEL
SILICON
ε (π mm mrad (MeV)^½)
PERCENTAGE OF TOTAL NEGATIVE ION BEAM INTENSITY
0
1
2
3
4
5
6
7
8
9
10
0
10
20
30
40
50
60
70
80
90
100

Fig. 9

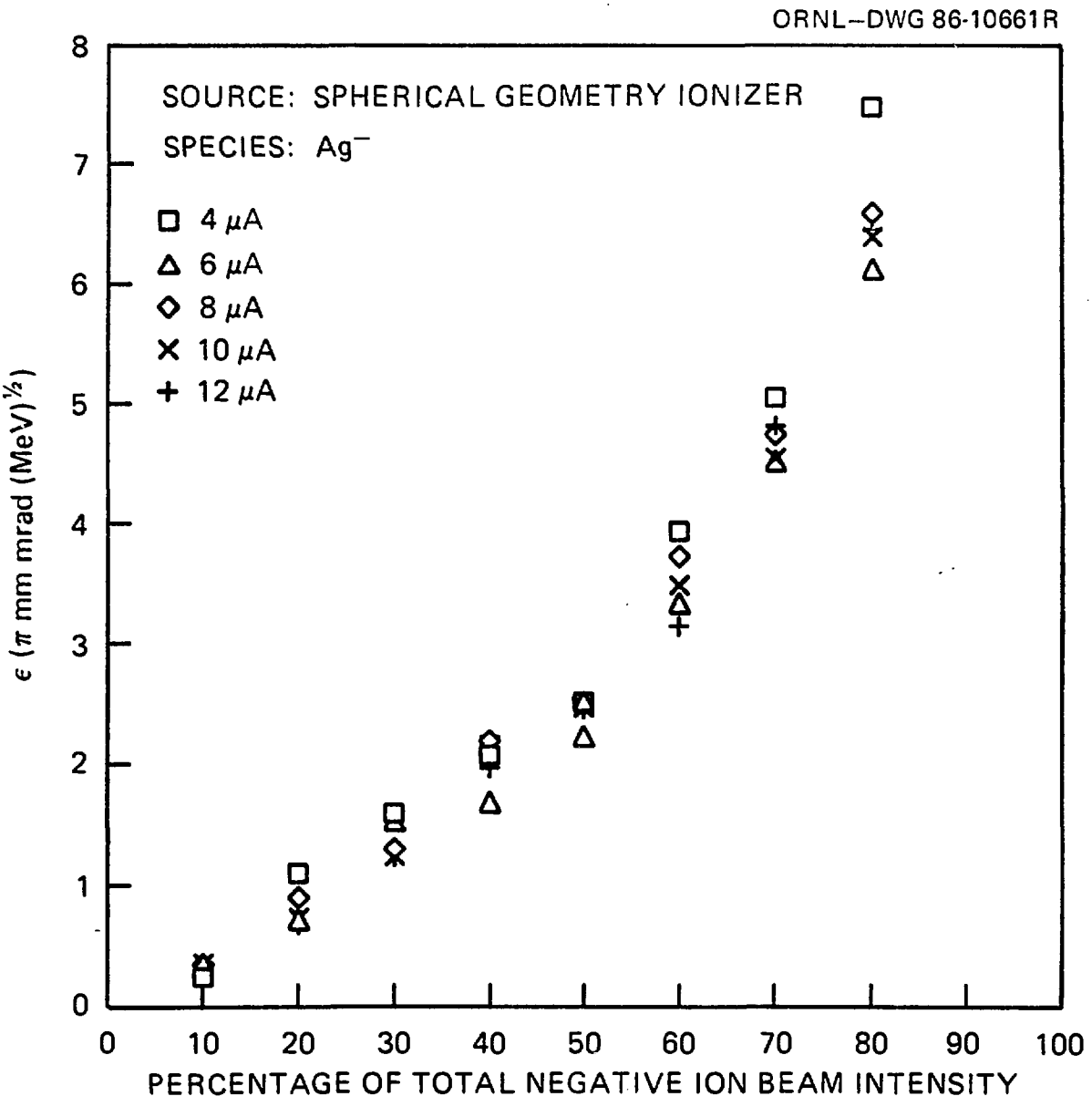
ORNL–DWG 86-10661R
SOURCE: SPHERICAL GEOMETRY IONIZER
SPECIES: Ag⁻
4 μA
6 μA
8 μA
10 μA
12 μA
ε (π mm mrad (MeV)^½)
PERCENTAGE OF TOTAL NEGATIVE ION BEAM INTENSITY
0
1
2
3
4
5
6
7
8
0
10
20
30
40
50
60
70
80
90
100

Fig. 10

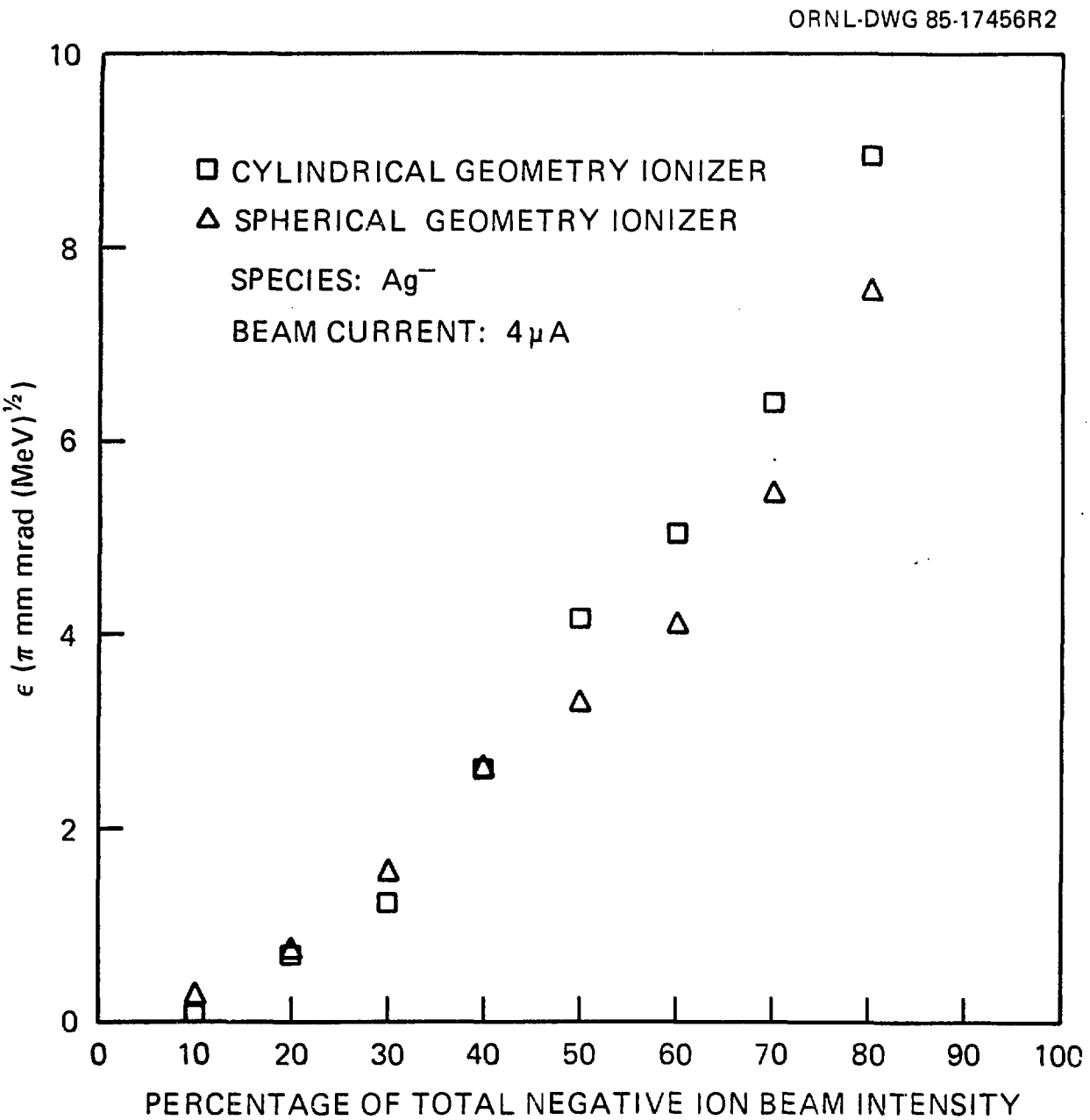
ORNL-DWG 85-17456R2
CYLINDRICAL GEOMETRY IONIZER
SPHERICAL GEOMETRY IONIZER
SPECIES: Ag⁻
BEAM CURRENT: 4 μA
ε (π mm mrad (MeV)^½)
PERCENTAGE OF TOTAL NEGATIVE ION BEAM INTENSITY
0
2
4
6
8
10
0
10
20
30
40
50
60
70
80
90
100

Fig. 11